

# Global HRTF Interpolation via Learned Affine Transformation of Hyper-conditioned Features

Jin Woo Lee, Sungho Lee, and Kyogu Lee

Music and Audio Research Group (MARG), Seoul National University, South Korea  
 {jinwlee, sh-lee, kglee}@snu.ac.kr

## Abstract

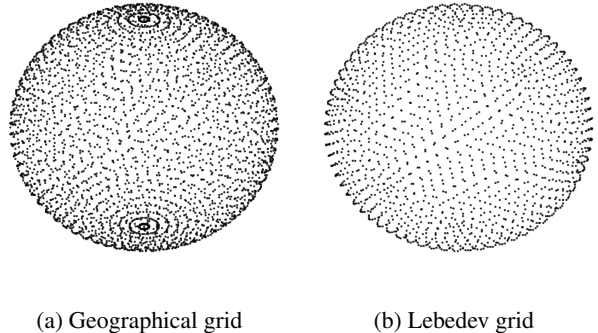
Estimating Head-Related Transfer Functions (HRTFs) of arbitrary source points is essential in immersive binaural audio rendering. Computing each individual’s HRTFs is challenging, as traditional approaches require expensive time and computational resources, while modern data-driven approaches are data-hungry. Especially for the data-driven approaches, existing HRTF datasets differ in spatial sampling distributions of source positions, posing a major problem when generalizing the method across multiple datasets. To alleviate this, we propose a deep learning method based on a novel conditioning architecture. The proposed method can predict an HRTF of any position by interpolating the HRTFs of known distributions. Experimental results show that the proposed architecture improves the model’s generalizability across datasets with various coordinate systems. Additional demonstrations using coarsened HRTFs demonstrate that the model robustly reconstructs the target HRTFs from the coarsened data.

**Index Terms:** head-related transfer functions, deep learning, interpolation, spatial audio

## 1. Introduction

Humans can localize sound using a variety of perceptual cues, including interaural time difference, interaural level difference, and spectral shifts in the source signal caused by interactions with the pinnae, head, and torso of the listener [1, 2]. Head-Related Transfer Function (HRTF) models the spectral changes in acoustic signals as they travel from a sound source to the listener’s ears. Since the anthropometric measurements are different for each listener, measuring HRTFs is essentially an individualized estimation. Once the HRTFs for a subject are obtained, virtual auditory space can be created by filtering a source sound with the transfer functions that correspond to the subject’s spectral cues. By presenting the filtered sound through headphones, one can give the listener the perception that the sound is localized at the desired virtual space [3]. Methods for finding out the HRTFs of each individual have been widely studied [4, 5].

Traditionally, numerical simulations that solve the wave equation are performed to obtain HRTFs for a given head mesh. The boundary element method (BEM) [6, 7] and finite element method (FEM) [8, 9] are commonly used. Brinkmann et al. [10] presented temporal and spectral analyses of their numerical method based on the BEM accelerated by the fast multipole method [11], comparing with their measurement [12, 13]. They reported that the measured and simulated HRTFs show good agreement and provided a solution to correct inaccuracies presumably caused by the mechanical setup. Despite several



(a) Geographical grid

(b) Lebedev grid

Figure 1: Two distributions of grid points indicating positions of point sources used in HRTF measurements/simulations. (a) Geographical grid contains same number of points for each elevation and azimuth. (b) In Lebedev grid, the number of points within a plane changes for varying the elevation or azimuth degrees. Different grid configuration for each dataset motivates a flexible interpolation method.

acceleration techniques have been proposed [14, 15], numerical analysis approaches have their limitation in that they require higher computational costs, compared to data-driven methods.

Recently, data-driven methods for binaural synthesis have been widely studied [16, 17, 18, 19]. These methods inherently require a sufficiently large number of data points to estimate the distribution of interest. HUTUBS dataset [20] is the largest among fully-public HRTF datasets [21]; it provides both measured and simulated HRTFs along with anthropometric measurements. However, the number of subjects within the HUTUBS dataset is still insufficient to split the dataset for the usual validation of the methods [17]. Therefore, in order to increase the number of training data, Chen et al. [22] combined three datasets. Furthermore, in order to combine the dataset of different coordinate systems, they applied a mapping rule, which is inapplicable for the elevation angles other than 0 [22].

To this end, we propose a method to resolve the problem of incorporating HRTF datasets of different coordinate systems. The proposed method predicts an HRTF of the desired position from neighboring known HRTFs with their corresponding positions and anthropometric measurements. Using position-aware interpolation within a local region of interest, our model is more precise and robust in the difference of coordinate systems compared to linear interpolation. We also show that our conditioning method advantage generalization under limited numbers of anthropometric and positional data.

Code and models are available at: <https://github.com/jin-woo-lee/hrtf-interpolation>

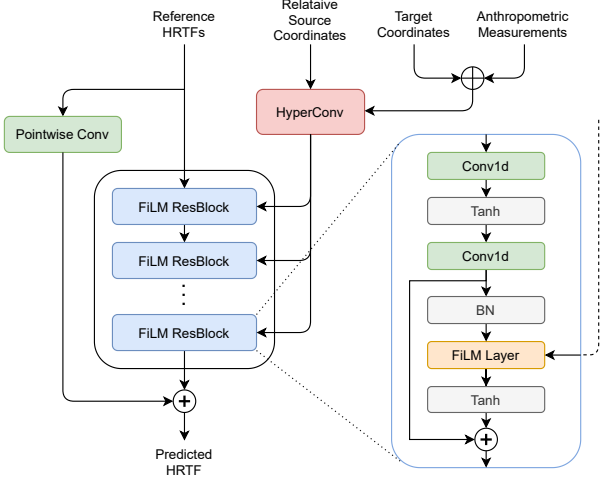


Figure 2: Block diagram of the proposed neural network architecture. The  $\oplus$  operator and  $+$  inside a circle denote the vector concatenation and element-wise addition, respectively.

## 2. Problem Statement

Our main objective is to obtain HRTFs of unseen emitter positions by transforming the available reference HRTFs with a neural network conditioned on physical features. Fast Fourier Transform (FFT) of a sufficient-length HRIR represents the HRTF well, so we borrow the term ‘‘HRTF’’ to denote the FFT.

Now, let  $X_p^{(a)} \in \mathbb{R}^K$  be a HRTF with emitter position  $p$  and anthropometric measurements  $a \in \mathbb{R}^J$  ( $K$  denotes the number of FFT frequency bins). Furthermore, let  $\mathcal{X}^{(a)}$  be the collection of HRTF data from a subject  $a$ , containing responses from source points located in various positions. Define a set of the source positions of the dataset  $\mathcal{X}^{(a)}$  as

$$\mathbf{p}^{(a)} = \left\{ p \in \mathbb{R}^3 : X_p^{(a)} \in \mathcal{X}^{(a)} \right\} \quad (1)$$

represented in Cartesian coordinates. The HRTF can either be a numerically calculated or a experimentally measured. Assume that we aim to retrieve an HRTF from a position  $p \in \mathbb{R}^3$ . First, we define a set of neighbors of  $p$  with known measurements as

$$\mathbf{n}_p = \{q \in \mathbf{p}^{(a)} : 0 < d_E(q, p) < \delta\} \quad (2)$$

where  $d_E$  represents the Euclidean distance. Then, we aim to find a function  $\Phi$  which takes the neighbor measurements  $X_{q_1}^{(a)}, \dots, X_{q_N}^{(a)}$  and positions  $q_1, \dots, q_N \in \mathbf{n}_p$  as input and estimates an HRTF of the target position  $p$  as follows,

$$\Phi_\theta : (X_q^{(a)}, q, p, a) \mapsto \hat{X}_p^{(a)} \in \mathbb{R}^K. \quad (3)$$

Here,  $q = \tilde{q}_1 \oplus \dots \oplus \tilde{q}_N$  denotes the concatenated tensors of the neighbor positions  $\tilde{q}_i = q_i - p$  to the target.  $X_q^{(a)} = X_{q_1}^{(a)} \oplus \dots \oplus X_{q_N}^{(a)}$  is the concatenated HRTFs. The neural network parameter  $\theta$  is updated to minimize the error

$$\sum_{a \in \mathbf{a}} \sum_{p \in \mathbf{p}^{(a)}} \mathcal{L} \left( X_p^{(a)}, \Phi_\theta(X_q^{(a)}, q, a) \right) \Big|_{q \sim \mathbf{n}_p} \quad (4)$$

with respect to the metric  $\mathcal{L}$ . We may restrict the target point  $p$  within the set  $\mathbf{p}^{(a)}$  to solve the problem in supervised learning setting.

## 3. Proposed Method

### 3.1. Network architecture

Our network (see Figure 2) is built upon Feature-wise Linear Modulation (FiLM) [23], an architecture designed for general-purpose conditioning. First, we used a pointwise convolution block (PC) that interpolate input HRTFs by linear combination with learned coefficients. The resultant HRTF is calibrated by the output from a stacks of FiLM residual blocks, of which we refer to as FiLM. Input signals of each FiLM layer (FiLM Layer) are scaled and biased by learned vectors calculated from affine transformation of conditioning vectors. In order to utilize the coordinates  $p, q$ , and the anthropometric measurements  $a$  as a conditioning vector, we used sinusoidal embedding [24] with the encoding dimension equal to the number of frequency bins  $K$ .

Yet, the number of anthropometric data within an HRTF dataset is equal to the number of subjects, it is comparably smaller than the number of coordinates, or that of the HRTFs. Since the number of subjects are often insufficient for data-driven methods, the neural networks are likely to be overfitted to the  $a$ . Therefore, other than choosing a naïve concatenation of  $p, q$ , and  $a$  as the condition of FiLM Layer, an additional conditioning method was employed. We introduce a new architecture that modulates the conditions for FiLM Layer using a hyper-convolution layer (HyperConv). The HyperConv convolve its inputs using weight and bias tensors calculated from its conditions. Conditioned by the anthropometric measurements and the target position, the HyperConv modulates the relative positions of the input HRTFs to generate conditions for the FiLM Layer. We hypothesize that this conditioning framework advantages generalized prediction of HRTFs.

**Feature-wise Linear Modulation.** The FiLM Layer consists of 5 stacked FiLM residual blocks [23]. We used 1D convolution with kernel size 3 instead of 2D convolution that appears in [23]. The first convolution layer of the first FiLM residual block expands the number of channels from  $N$  to  $4N$ , and the first convolution layer of the last FiLM residual block reduce the number of channels from  $4N$  to 1. For the other convolution layers, the number of channels remained constant. Additionally, we used the tanh activation instead of the ReLU activation so that the training with the dB-scaled input is stable. We formulate our feature-wise affine map for the given input signal  $x_{1:K} \in \mathbb{R}^{C_{\text{in}} \times K}$  and the conditioning signal  $c_{1:K} \in \mathbb{R}^{1 \times K}$  as

$$z_{j,:} = \mathcal{F}^{(\gamma)}(c)_j \cdot x_{j,:} + \mathcal{F}^{(\beta)}(c)_j \quad (5)$$

where  $\mathcal{F}^{(\gamma)}$  and  $\mathcal{F}^{(\beta)}$  denote linear operators.

**Hyper-convolution.** The hyper-convolution layer is a linear module of which the weights and biases are generated from given conditions. In the work by [25, 19], the hyper-convolution was used for conditioning the temporal convolutional network that operates in the time domain. We adopt a similar setting with [25], yet without dilation and different kernel size, since our HyperConv deals with encoded positions and anthropometric features. Following the formulation of [25], we express our hyper-convolution of the given input signal  $x \in \mathbb{R}^{C_{\text{in}} \times K}$  and the conditioning signal  $c \in \mathbb{R}^{C_{\text{cond}} \times K}$  as

$$z_{:,k} = \sum_{i=0}^{\kappa-1} \left[ \mathcal{H}^{(w)}(c_{:,k}) \right]_{:,i} x_{:,k+i-\lfloor \kappa/2 \rfloor} + \mathcal{H}^{(b)}(c_{:,k}) \quad (6)$$

where  $\kappa$  is analogous to the kernel size of usual convolution operation, and  $\mathcal{H}^{(w)}$  and  $\mathcal{H}^{(b)}$  are small convolutional hyper-networks.

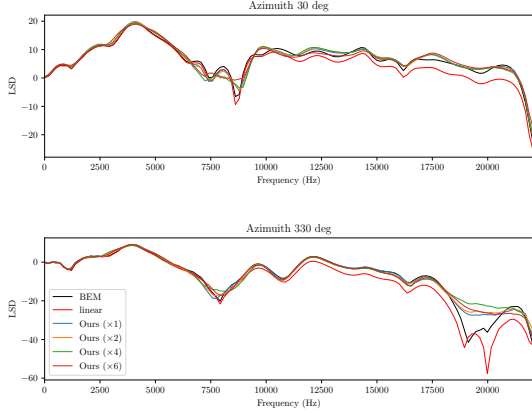


Figure 3: LSD evaluation of the proposed methods and linear interpolation baseline for azimuth 30°(top) and azimuth 330°(bottom).

## 4. Experiments

### 4.1. Data

We used the HUTUBS dataset [20] for the experiment, which consists of a total 96 number of distinct subjects. A total of 93 number of subjects were studied by excluding three subjects (with IDs 18, 79, and 92) whose anthropometric data are unavailable. The simulated HRTFs consist of a Lebedev grid with 1730 points. We transformed each provided 256-sample HRIR into the 129-sample HRTF points via FFT. We used 12 anthropometric features of the left ear measurements of each subject.

In order to test our model’s interpolation capability for data under a coordinate system other than the Lebedev grid, we evaluated the model with the FABIAN dataset [26], which uses geographical grid. The dataset measured and simulated HRTFs using both head and torso models, and one of the purposes of establishing the dataset includes analysis of changes in HRTF for various head-above-torso-orientation (HATO) degrees. Yet, we emphasize that the main feature of the FABIAN is that it provides high-resolution HRTFs, and we verify the generalization of our model for simulated HRTF with 0 HATO degree. Each simulated HRTF of the dataset consists of 11950 source positions with 2° in elevation, 2° great circle distance in azimuth. We also tested the model performance on coarsened FABIAN data, so the model reconstructs the ground truth with provided downsampled HRTFs.

### 4.2. Training

While training our model, we uniformly sampled with replacement of  $N$  source coordinates for each target point  $p$  from the neighborhood set  $\mathbf{n}_p$ . In the test phase, we sampled  $N$  closest source from the target in order to assess the best achievable performance, except for the the circumstances that  $|\mathbf{n}_p|$  is smaller than  $N$ . To train our network, we adopted log-spectral distance (LSD) as the minimization criteria, defined by a root-mean-squared error (RMSE) between the estimated and ground-truth log magnitudes. AdamW [27] was used as an optimizer, with a batch size of 64. The initial learning rate was set 0.0001 with  $\beta_1 = 0.9$  and  $\beta_2 = 0.999$ , and the learning rate was halved if three epochs have passed without improvement. We employed the 5-fold cross-validation, and no overfitting was detected.

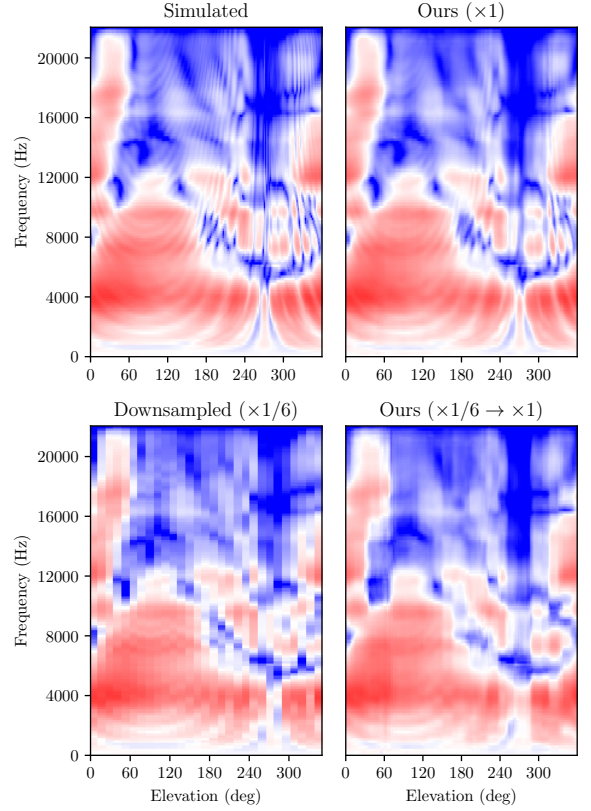


Figure 4: Comparison between simulated HRTF of median plane of FABIAN [26] (top left), estimated output of our model (top right), simulated HRTF of median plane of FABIAN downsampled by a factor of  $\frac{1}{6}$  (bottom left), and reconstruction by our model with provided the downsampled data (bottom right).

### 4.3. Ablation study

We conducted an ablation study on our best model to understand how the network learns interpolation by conditioning the physical features. We report the models with  $N = 8$  in  $\delta = 0.3$  on HUTUBS in Table 1. Beginning from the case of using only the pointwise convolution (PC) as a baseline, we added the FiLM residual network (FiLM), or additionally used FiLM layer (FiLM Layer) or hyper-convolution layer (HyperConv) in order to condition FiLM. The baseline (a) is equivalent to a linear operation that superposition the input HRTFs with learned coefficients. No conditioning method was adopted in the baseline. For (b), we used similar architecture of FiLM network as proposed in [23], and conditioned the concatenated vectors of encoded positions and anthropometric features. We further hypothesized that the condition which inform the positions of input HRTFs should be modulated by the position of target HRTF and anthropometric features, as illustrated by red box in Figure 2. Table 1 (c1) and (c2) show the result of using different conditioning methods for modulating the conditions. In (c1), FiLM residual block (single blue box in Figure 2) with kernel size 1 was utilized for modulating the conditions. Using the conditioning method as (c2) advantaged the most accurate interpolation of HRTFs. We empirically observed that hyper-convolution advantages conditioning the physical features in predicting HRTFs.

Table 1: Comparison of average log-spectral distortion for all directions depending on the modules used for training.

Model	LSD
(a) PC	1.875
(b) PC + FiLM	1.767
(c1) PC + FiLM + FiLM Layer	1.767
(c2) PC + FiLM + HyperConv	<b>1.736</b>

Table 2: Comparison of average LSD on test set of HUTUBS.

Method	All	Hor.	Med.	Fro.
Linear Interp.	6.538	6.418	2.289	6.842
Ours, $\delta = 0.2$	<b>1.761</b>	<b>2.093</b>	<b>1.139</b>	<b>2.198</b>

#### 4.4. Results

We compared our model with a baseline which linearly interpolates the two closest samples within a plane of equal azimuth or elevation. We denote the horizontal/median/frontal plane by ‘Hor.’/‘Med.’/‘Fro.’, respectively. Average result for the samples of every azimuth/elevation angle is denoted by ‘All’.

**Interpolation.** Table 2 compares average performance of our model with  $N = 16$  and  $\delta = 0.2$  with the linear interpolation baseline. Our method outperformed the baseline for all directions and every planes. In the Lebedev grid, it is difficult to find planes that make the distances between points densely distributed. Because of this, linear interpolation was easy to fail in HUTUBS. On the other hand, linear interpolation of the FABIAN dataset [26] showed comparably better performance than the linear interpolation result in HUTUBS. Table 3 shows the performance of our model, which was trained using HUTUBS and tested using simulated HRTF in FABIAN. Although the tested HRTFs are aligned in unseen coordinate system and radius, our model performed similar to the result observed in HUTUBS. The model also outperformed the baseline for horizontal and median planes, and the LSD averaged for all directions.

**Super-resolution.** We also tested our model’s interpolation performance under more coarsened HRTF grids by factor of  $1/T$ . In order to assure the existence of input points within the neighborhood  $\mathbf{n}_p$ , we show the performance of our model trained using  $N = 16$  within  $\delta = 0.6$ , even though the model is not the best one of our analysis. Table 3 shows average LSD of our model with provided reference HRTFs uniformly coarsened by factor of  $1/2$ ,  $1/4$ , or  $1/6$ . Although given only  $1/6$  times less data compared to the original, our model maintained generally better performance than the baseline. For the plotted results of super-resolution task, we refer to Figure 4. Since we could not sample enough  $N$  data within the  $\delta$  of our model, the measured HRTFs of FABIAN dataset could not be tested.

Table 3: Comparison of average LSD tested using FABIAN dataset [26].

Method	All	Hor.	Med.	Fro.
Linear Interp.	2.539	3.145	3.245	<b>2.071</b>
Ours, $\delta = 0.6$	<b>1.897</b>	<b>2.190</b>	<b>1.686</b>	2.514
Ours ( $\times 1/2$ )	2.105	2.481	2.414	3.000
Ours ( $\times 1/4$ )	2.353	2.806	2.775	3.280
Ours ( $\times 1/6$ )	2.513	2.941	2.861	3.269

borhood  $\mathbf{n}_p$ , we show the performance of our model trained using  $N = 16$  within  $\delta = 0.6$ , even though the model is not the best one of our analysis. Table 3 shows average LSD of our model with provided reference HRTFs uniformly coarsened by factor of  $1/2$ ,  $1/4$ , or  $1/6$ . Although given only  $1/6$  times less data compared to the original, our model maintained generally better performance than the baseline. For the plotted results of super-resolution task, we refer to Figure 4. Since we could not sample enough  $N$  data within the  $\delta$  of our model, the measured HRTFs of FABIAN dataset could not be tested.

**Setting neighborhood.** Figure 5 shows the average performance of the models trained with different neighborhood constraints. We explored appropriate size  $\delta$  and number of sampling points  $N$  of the neighborhood  $\mathbf{n}_p$  using the test set of HUTUBS. The LSD increased for all models with increment in the neighborhood radius  $\delta$  when the number of sampling points is fixed. For sufficiently small  $\delta$ , the error decreased when more points were sampled. However, the models trained with  $N = 8$  consistently performed better than the others for  $\delta \geq 0.3$ . Models trained with larger  $\delta$  get less chance to be provided with necessary cues in predicting the HRTFs of target position while training. Thus training models with larger  $\delta$  involve higher difficulties of optimizing the model. However, we empirically observed that the models trained using larger  $\delta$  generalized better, especially for upsampling with large scales.

## 5. Conclusion

In this work, we introduced a neural network that interpolates given HRTFs by conditioning source positions and anthropometric measurements. We explored the use of two conditioning methods, FiLM and hyper-convolution, for our network that estimate the HRTF of the desired position for given HRTFs sampled from its neighborhood. Quantitative analysis showed that our method precisely interpolates the HRTFs, outperforming the baseline. The ablation experiment showed that the proposed conditioning method performed better than the rest of the experimented methods. Also, the model with the proposed conditioning scheme generalized well to the unseen dataset with the unseen grid system. Furthermore, we demonstrated that our network is able to reconstruct the downsampled HRTFs. We expect future developments in personalized HRTF generation based on the proposed system.

## 6. Acknowledgement

This work was supported by Electronics and Telecommunications Research Institute(ETRI) grant funded by the Korean government.[22ZH1200, The research of the basic media-contents technologies]

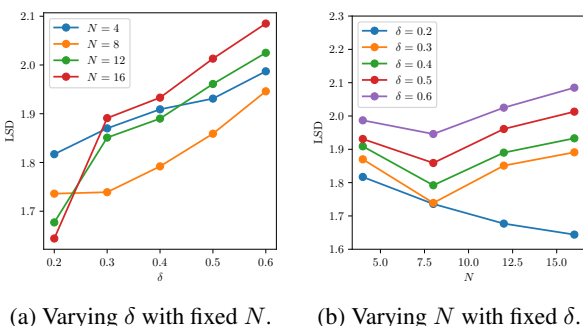


Figure 5: Comparison of model performance for the radius  $\delta$  and the number of sampling points  $N$  within the neighborhood  $\mathbf{n}_p$ .

## 7. References

- [1] D. Wright, J. H. Hebrank, and B. Wilson, "Pinna reflections as cues for localization," *The Journal of the Acoustical Society of America*, vol. 56, no. 3, pp. 957–962, 1974.
- [2] F. Asano, Y. Suzuki, and T. Sone, "Role of spectral cues in median plane localization," *The Journal of the Acoustical Society of America*, vol. 88, no. 1, pp. 159–168, 1990.
- [3] C. Hendrix and W. Barfield, "The sense of presence within auditory virtual environments," *Presence: Teleoperators & Virtual Environments*, vol. 5, no. 3, pp. 290–301, 1996.
- [4] S. Li and J. Peissig, "Measurement of head-related transfer functions: A review," *Applied Sciences*, vol. 10, no. 14, p. 5014, 2020.
- [5] S. Xu, Z. Li, and G. Salvendy, "Individualization of head-related transfer function for three-dimensional virtual auditory display: a review," in *International Conference on Virtual Reality*. Springer, 2007, pp. 397–407.
- [6] B. F. Katz, "Boundary element method calculation of individual head-related transfer function. i. rigid model calculation," *The Journal of the Acoustical Society of America*, vol. 110, no. 5, pp. 2440–2448, 2001.
- [7] W. Kreuzer, P. Majdak, and Z. Chen, "Fast multipole boundary element method to calculate head-related transfer functions for a wide frequency range," *The Journal of the Acoustical Society of America*, vol. 126, no. 3, pp. 1280–1290, 2009.
- [8] N. A. Gumerov, R. Duraiswami, and Z. Tang, "Numerical study of the influence of the torso on the hrtf," in *2002 IEEE International Conference on Acoustics, Speech, and Signal Processing*, vol. 2. IEEE, 2002, pp. II–1965.
- [9] T. Xiao and Q. Huo Liu, "Finite difference computation of head-related transfer function for human hearing," *The Journal of the Acoustical Society of America*, vol. 113, no. 5, pp. 2434–2441, 2003.
- [10] F. Brinkmann, A. Lindau, M. Müller-Trapet, M. Vorländer, and S. Weinzierl, *Cross-validation of measured and modeled head-related transfer functions*, 2015.
- [11] A. Lindau, T. Hohn, and S. Weinzierl, "Binaural resynthesis for comparative studies of acoustical environments," in *Audio Engineering Society Convention 122*. Audio Engineering Society, 2007.
- [12] F. Brinkmann, A. Lindau, S. Weinzierl, G. Geissler, and S. van de Par, *A high resolution head-related transfer function database including different orientations of head above the torso*, 2013.
- [13] J. Otten, "Factors influencing acoustical localization," Ph.D. dissertation, Universität Oldenburg, 2001.
- [14] N. Raghuvanshi, R. Narain, and M. C. Lin, "Efficient and accurate sound propagation using adaptive rectangular decomposition," *IEEE Transactions on Visualization and Computer Graphics*, vol. 15, no. 5, pp. 789–801, 2009.
- [15] J.-H. Wang and D. L. James, "Kleinpat: optimal mode conflation for time-domain precomputation of acoustic transfer," *ACM Trans. Graph.*, vol. 38, no. 4, pp. 122–1, 2019.
- [16] M. Zhang, J.-H. Wang, and D. L. James, "Personalized hrtf modeling using dnn-augmented bem," in *ICASSP 2021-2021 IEEE International Conference on Acoustics, Speech and Signal Processing (ICASSP)*. IEEE, 2021, pp. 451–455.
- [17] Y. Wang, Y. Zhang, Z. Duan, and M. Bocko, "Global hrtf personalization using anthropometric measures," in *Audio Engineering Society Convention 150*. Audio Engineering Society, 2021.
- [18] Y. Zhou, H. Jiang, and V. K. Ithapu, "On the predictability of hrtfs from ear shapes using deep networks," in *ICASSP 2021-2021 IEEE International Conference on Acoustics, Speech and Signal Processing (ICASSP)*. IEEE, 2021, pp. 441–445.
- [19] I. D. Gebru, D. Marković, A. Richard, S. Krenn, G. A. Butler, F. De la Torre, and Y. Sheikh, "Implicit hrtf modeling using temporal convolutional networks," in *ICASSP 2021-2021 IEEE International Conference on Acoustics, Speech and Signal Processing (ICASSP)*. IEEE, 2021, pp. 3385–3389.
- [20] F. Brinkmann, M. Dinakaran, R. Pelzer, J. Wohlgemuth, F. Seipl, and S. Weinzierl, "The hutubs hrtf database," *DOI*, vol. 10, p. 14279, 2019.
- [21] C. Guezenoc and R. Seguier, "A wide dataset of ear shapes and pinna-related transfer functions generated by random ear drawings," *The Journal of the Acoustical Society of America*, vol. 147, no. 6, pp. 4087–4096, 2020.
- [22] T.-Y. Chen, T.-H. Kuo, and T.-S. Chi, "Autoencoding hrtfs for dnn based hrtf personalization using anthropometric features," in *ICASSP 2019-2019 IEEE International Conference on Acoustics, Speech and Signal Processing (ICASSP)*. IEEE, 2019, pp. 271–275.
- [23] E. Perez, F. Strub, H. De Vries, V. Dumoulin, and A. Courville, "Film: Visual reasoning with a general conditioning layer," in *Proceedings of the AAAI Conference on Artificial Intelligence*, vol. 32, no. 1, 2018.
- [24] A. Vaswani, N. Shazeer, N. Parmar, J. Uszkoreit, L. Jones, A. N. Gomez, Ł. Kaiser, and I. Polosukhin, "Attention is all you need," in *Advances in neural information processing systems*, 2017, pp. 5998–6008.
- [25] A. Richard, D. Markovic, I. D. Gebru, S. Krenn, G. A. Butler, F. Torre, and Y. Sheikh, "Neural synthesis of binaural speech from mono audio," in *International Conference on Learning Representations*, 2020.
- [26] F. Brinkmann, A. Lindau, S. Weinzierl, M. Müller-Trapet, R. Opdam, M. Vorländer *et al.*, "A high resolution and full-spherical head-related transfer function database for different head-above-torso orientations," *Journal of the Audio Engineering Society*, vol. 65, no. 10, pp. 841–848, 2017.
- [27] S. J. Reddi, S. Kale, and S. Kumar, "On the convergence of adam and beyond," *arXiv preprint arXiv:1904.09237*, 2019.